



Topology of voids and channels in selected porphyrinic compounds

Lawrence P. Cook ^{1,2,a)} Greg A. Brewer,¹ Daniel Siderius,³ and Winnie Wong-Ng ⁴¹Department of Chemistry, The Catholic University of America, Washington, DC 20064, USA²Materials Science and Engineering Program, The Catholic University of America, Washington, DC 20064, USA³Chemical Science Division, The National Institute of Standards and Technology, Gaithersburg, MD 20899, USA⁴Materials Measurement Science Division, The National Institute of Standards and Technology, Gaithersburg, MD 20899, USA

(Received 10 August 2019; accepted 22 August 2019)

Porphyrinic compounds are of increasing interest to the materials science community, yet little attention has been paid to crystallographically controlled voids and channels in these materials. We have conducted an initial survey of the voids and channels in a random subset of 1000 porphyrinic compounds with known crystal structures. From calculations using a rolling-probe subroutine, we have found that about 5% of these compounds have line-of-sight channels, which differ in their topology depending on the crystallography. A small but significant number of porphyrinic compounds have calculated void contents of >25 volume %. We discuss in detail the void and channel characteristics, including pore-size distribution, of four representative compounds, with technological implications. © 2019 International Centre for Diffraction Data. [doi:10.1017/S0885715619000770]

Key words: porphyrins, voids, channels, pore-size distribution, topology

I. INTRODUCTION

Porphyrins have a long and continuing history of scientific investigation, which has been chronicled in various reviews and compilations, most notably the Handbook of Porphyrin Science, the latest version of which has been expanded to include 45 volumes (Kadish *et al.*, 2010–2019). Much of the literature has to do with porphyrins in solution; however, increasingly, they have become of interest as functional materials in the solid state as a result of their chemical versatility and range of properties (Suslick *et al.*, 2000; Galloni *et al.*, 2014; Cook *et al.*, 2016, 2017; Jiang and Sun, 2019). Typically, porphyrins have greater chemical and thermal stability than many organic materials. Furthermore, because of their solubilities, for many of these compounds, it is realistic to think in terms of developing relatively low-cost solution-processing routes. This is especially relevant for thin-film applications, including electronic devices which capitalize on the relatively flexible nature of organic materials.

The basic chemistry of the porphyrin structure is shown schematically in Figure 1. The essential features include a macrocycle comprised of four linked pyrrole heterocycles, which allows for metalation of the central cavity of the macrocycle by deprotonation and bonding to the four internal nitrogen atoms. Additionally, a large variety of substituents may be linked to the carbons at either the β or the *meso* external positions of the macrocycle. The porphyrin macrocycle is an aromatic structure which may be conjugated to other porphyrin molecules through π -bonding or conjugated to attached aromatic substituents, thus giving rise to interesting semiconducting properties (Jones *et al.*, 1984; Crossley and Burn, 1991; Jurow *et al.*, 2010). Mononuclear porphyrins exhibit basically planar structures but are known to undergo structural

distortions that include twisting, doming, ruffling, and bending. Poly-porphyrinic compounds can exhibit even greater structural variations.

In this paper, we consider the crystallography and crystal chemistry of selected porphyrinic compounds with regard to their intrinsic micro-porosity. Porosity, which includes the presence of both closed and open voids (channels), is of great importance for many applications. By combining porosity with porphyrin properties at the molecular level, the range of functionalities can be significantly expanded.

II. METHODS

We have identified over 8000 porphyrinic compounds with known crystal structures based on an automated search of the Cambridge Crystal Data Centre (CCDC) organic database (Cambridge Crystallographic Data Centre, 2019), using as a search criterion, the presence within the structure of the moiety shown in Figure 1. A systematic study of void topologies in this group of materials, an important characteristic, has not been previously completed, as the required software has only recently become available. As an initial effort in this direction, we have examined a randomly selected subset of 1000 structures with regard to the presence of voids. For this subset, void surface geometries and void volume percentages were calculated based on the crystal data using Mercury 4.1.0 (Cambridge Crystallographic Data Centre, 2019) via a rolling-ball structure probe subroutine in which the contact surface of the probe with the constituent atoms, defined in terms of their van der Waals radii, is mapped out. (The purpose of identifying equipment and software packages in this article is to specify the experimental procedure. Such identification does not imply recommendation or endorsement by the National Institute of Standards and Technology.) For these preliminary calculations, in which compounds were screened for relatively high volume % of voids, a probe radius of 1.2 Å

^{a)} Author to whom correspondence should be addressed. Electronic mail: cooklp@cua.edu

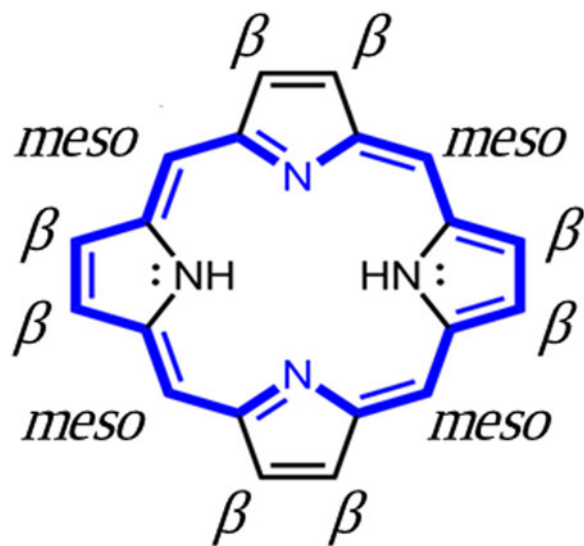


Figure 1. Structure of the porphyrin macrocycle, showing β and *meso* substituent bonding sites. Blue = π -bonding network.

[the van der Waals radius of the non-bonded hydrogen atom (Bondi, 1964)] was used.

More detailed characterizations were carried out for compounds selected from among the high-void-volume percentage results. These characterizations were completed using computational techniques to estimate the gas-accessible pore volume and porosity, the surface area, and the pore-size distribution (PSD). The geometric techniques chosen (Gelb and Gubbins, 1999; Frost *et al.*, 2006; Duren *et al.*, 2007; Palmer *et al.*, 2011) have already been used and described in other works by some of the present authors (Wong-Ng *et al.*, 2012, 2013, 2015, 2018, 2019; Nguyen *et al.*, 2019). The same atomic radii (Bondi, 1964; Rowland and Taylor, 1996) were used for consistency with previous PSD estimations. According to Walton and Snurr (2007), the geometric estimations of the surface area should approximate experimental BET measurements. For this and our previous work, the PSD is based on the concept of the “local pore size,” i.e., the local pore size at a particular position is equal to the diameter of the largest sphere that includes that position without eclipsing the material framework. Then, the PSD of a particular pore diameter is simply the fraction of the free pore volume with local pore size equal to the selected diameter. In this definition, the PSD serves to estimate the free volume fraction belonging to cavities and channels according to the largest sphere that can fit in each structural feature. In the context of the present work, PSD estimations can serve to identify pore space that is not part of LOS channels, especially cavities that may be present between or in addition to channels.

III. RESULTS

As noted above, voids are of two basic types, closed and extended (i.e. channels). Voids which are closed are essentially unavailable for accepting molecules after crystallization, and may be empty, but also may contain guests incorporated and trapped at the time of crystallization. On the other hand, channels can provide continuous pathways into and out of the interior of the crystal, and are thus of greater interest for many materials applications. From our calculations on the

data subset of 1000 structures and the subsequent analysis of results, we observed that structures with a void content of more than 5–10 volume % are the most likely to have extended voids, i.e. continuous channels. This group comprised about 5% of the total. The continuous channels can either have unimpeded line-of-sight (LOS) character, or they may have extensive tortuosity which precludes an LOS character. We have determined whether continuous channels exist, and if they do, their basic topology, by completing the three-dimensional (3D) visual examination of each of the high-void-volume percentage candidates. Space does not permit a discussion of each of the promising compounds. Consequently, we have selected examples representing the range of characteristics encountered in compounds with LOS channels. Selections have been based partially on the absence of guests or if present, their characterization as part of the structure. Our examples have been selected from different crystal systems to illustrate the influence of crystallography on the topology of the continuous channels.

The values in Table I are kinetic diameters of common adsorbate gases, useful for comparison with estimated average channel diameters. Kinetic diameter expresses the likelihood that a molecule in gas will collide with another molecule. Kinetic diameter is related to the mean free path of molecules in a gas.

A. Cubic (*Im-3m*) tetracarboxyphenyl porphyrin (nickel II) zirconium metal-organic framework (PCN-202(Ni)-Zr) or (BEPVIE)

The data examined from the subset include (1) molecular compounds in which discrete porphyrin molecules are packed and held together by weak van der Waals bonds, hydrogen bonds, or electrostatic interactions, and (2) framework structures where the porphyrins serve as ionically bonded linkers. For the molecular structures, compounds with cubic symmetry are not as common, possibly because of the complexity of efficiently packing porphyrin molecules having sterically hindering substituents. The packing issue is mitigated in ionically bonded, porphyrin-linked metal-organic framework structures (MOFs), where higher symmetry is promoted by the presence of the symmetrically coordinated metal nodes. The structure of PCN-202(Ni)-Zr or BEPVIE, classified as an MOF, was determined by Yuan *et al.* (2018) (PCN stands for porous coordination network). Visualization of the compound’s complex structure is facilitated by comparison to that of the simpler, but similar structure of its precursor, PCN-224(Ni), whose framework is formed by eight 6-connected Zr_6 cuboctahedral clusters (with terminal H_2O/OH groups) positioned at the corners of a cubic cage, as shown diagrammatically in Figure 2.

In this precursor, the Zr_6 clusters are linked diagonally to one another by nickel-metalated tetrakis(4-carboxyphenyl) porphyrin at the centers of cube faces. PCN-202(Ni)-Zr is derived from this structure by adding disordered 4,4’-dicarboxydiphenyl sulfone (DCDPS) as a tritopic linker which allows insertion of another Zr_6 cluster at the cube centers. In this configuration, all the Zr_6 clusters are 12-connected (i.e. connected to other moieties by a total of 12 bonds). PCN-202(Ni)-Zr thus contains two structurally distinct types of 12-connected Zr_6 clusters, as well as disordered DCDPS linkers, and Ni^{2+} centered metalloporphyrin linkers. The

TABLE I. Dimensions of some adsorbate molecules (Breck, 1974; Li and Talu, 1993; Matteucci, *et al.*, 2006; Ismail *et al.*, 2015; Gao *et al.*, 2016).

Name	Formula	Kinetic diameter (Å)	Name	Formula	Kinetic diameter (Å)
Helium	He	2.60	Krypton	Kr	3.60
Ammonia	NH ₃	2.60	Nitrogen	N ₂	3.64
Water	H ₂ O	2.65	Carbon monoxide	CO	3.76
Neon	Ne	2.75	Methane	CH ₄	3.80
Hydrogen	H ₂	2.89	Ethylene	C ₂ H ₄	3.90
Nitric oxide	NO	3.17	Methanol	CH ₃ OH	3.95
Hydrogen chloride	HCl	3.20	Xenon	Xe	3.96
Chlorine	Cl ₂	3.20	Iodine	I ₂	~4
Acetylene	C ₂ H ₂	3.30	Propane	C ₃ H ₈	4.30
Carbon dioxide	CO ₂	3.30	Ethanol	C ₂ H ₅ OH	4.50
Nitrous oxide	N ₂ O	3.30	Propylene	C ₃ H ₆	4.50
Argon	Ar	3.40	Sulfur hexafluoride	SF ₆	5.50
Oxygen	O ₂	3.46	Benzene	C ₆ H ₆	5.85
Hydrogen bromide	HBr	3.50	Carbon tetrachloride	CCl ₄	5.90
Bromine	Br ₂	3.50	Cyclohexane	C ₆ H ₁₂	6.90
Hydrogen sulfide	H ₂ S	3.60			
Sulfur dioxide	SO ₂	3.60			

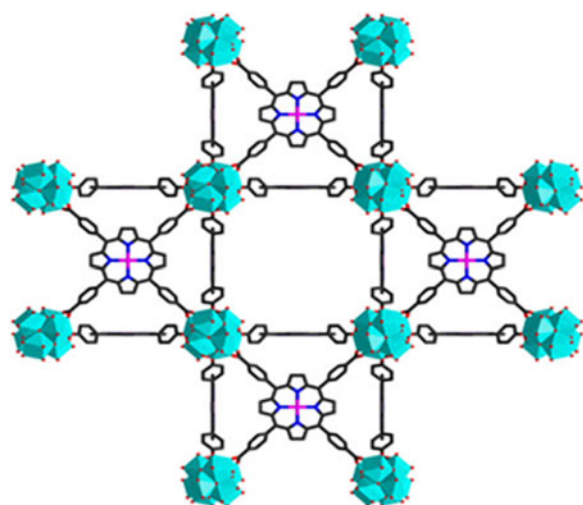


Figure 2. Structure of PCN-224(Ni), precursor to PCN-202(Ni)-Zr. Cyan = 6-connected Zr₆ clusters, magenta = nickel (Yuan *et al.*, 2018).

resulting structure for PCN-202(Ni)-Zr has a void volume % of 65.6%. The large void volume % results in a calculated density of 0.829 g cm⁻³. The void topology is shown in Figure 3 (a) in an inclined view approximately down [111], where the

three-fold axis of symmetry at the origin of the unit cell coordinates is evident.

The cubic symmetry results in an interconnected framework of voids extending in three equivalent dimensions throughout the structure, although as viewed along the *a*-axis in LOS cross section (Figure 3(b)), the oval channels appear somewhat restricted, at ~1.60 Å × ~7.35 Å. The compound exhibited experimental N₂ absorption of 600 cm³g⁻¹ (Yuan *et al.*, 2018), which confirms extensive access to the interior network of channels. The PSD in BEPVIE, which gives the relative abundance of various pore sizes, is shown in Figure 4. It has a strong peak centered at ~15.6 Å, reflective of the large volume which is not LOS. Additionally, the PSD identifies pores of diameters 4.8, 5.8, and 14 Å, the smaller of which are part of the LOS channels shown in Figure 3(b). In this instance, because of the relatively continuous and complex 3D network of internal channels and voids, the LOS channel cross-sections are not particularly indicative of the overall void topology. Most of the pores included in this PSD are not LOS channels, consistent with the fact that this is a framework structure with large equant or sub-equant interconnected internal cavities, rather than channels.

PCN-202(Ni)-Zr was shown to have excellent stability in aqueous solutions over a wide range of pH, attributed to the

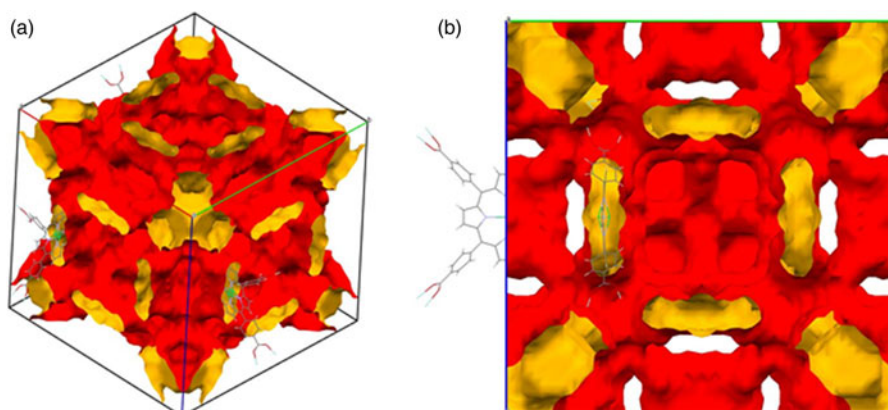


Figure 3. (a) Voids and channels in PCN-202(Ni)-Zr viewed approximately down [111]. Note: in this and subsequent figures, the inside of voids is indicated in red, the outside in yellow. (b) Voids and channels in PCN-202(Ni)-Zr unit cell viewed down the *a*-axis.

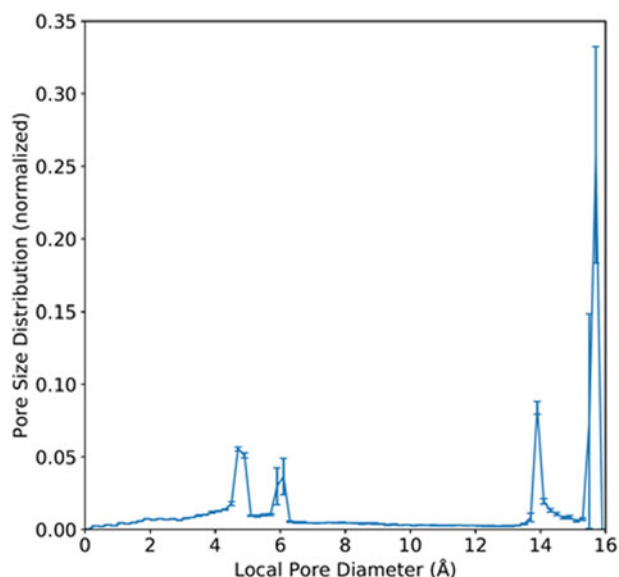


Figure 4. Pore-size distribution in BEPVIE. Uncertainty is indicated by error bars, which correspond to 95% confidence intervals on the mean PSD computed via jackknife analysis of 10 replicate calculations.

robustness of the Zr-carboxylate bond. It is thought that the presence of multiple metals favors increased catalytic activity, as observed in closely related compounds. Crystallographic data are summarized in Table II. The structure has a relatively large unit cell volume of $28\,351.39\text{ \AA}^3$, the same as the molecular volume.

B. Rhombohedral (*R*-3) pyridyldiphenyl zinc porphyrin (CAYROK)

The structure of the porphyrin CAYROK consists of a zinc-metalated macrocycle with pyridyl substituents at two opposing *meso* positions and phenyl substituents at the two other *meso* positions (Deiters *et al.*, 2005). Additionally, the

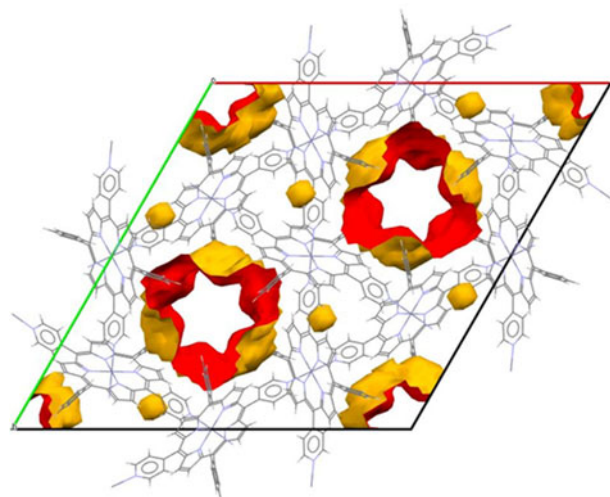


Figure 5. Voids and channels in CAYROK unit cell viewed down the *c*-axis.

Zn^{2+} at the center of the macrocycle is apically coordinated by two more pyridines. Although the basic macrocycle, including the zinc but excluding the substituents, is essentially planar, the coordination axis of the apical pyridines is not perpendicular to this plane, but rather is tilted at an angle of $\sim 69.9^\circ$. This feature produces a molecular packing which results in a hexagonal network with large LOS hexagonal channels along *c*, as shown in Figure 5. The void volume, which includes some smaller closed voids as well, is 18.1%. The minimum diameter of the star-shaped channels, as viewed on the LOS cross section along *c*, is $\sim 4.86\text{ \AA}$, and the maximum diameter (point-to-point of the star) is $\sim 6.65\text{ \AA}$. The pore-size distribution is shown in Figure 6. The large presence at slightly below 6 \AA correlates with the average diameter of the main LOS channels along *c*. The origin of the other peaks at lower diameters is not immediately clear from comparison with Figure 5; they may represent cavities on the main channel walls.

TABLE II. Crystal data for PCN-202(Ni)-Zr (Yuan *et al.*, 2018).

Common name	Tetracarboxyphenyl nickel porphyrin zirconium MOF
Common acronym	PCN-202(Ni)-Zr
CCDC symbol ^a	BEPVIE
IUPAC name ^a	Pentakis(tetrakis(μ -hydroxo)-(tetrakis(μ -oxido)-hexa(zirconium(IV))octadecakis(4,4',-(sulfanediy)l)dibenzoate hexakis((5,10,15,20-tetrakis(4-carboxylatephenyl)porphyrinato)-nickel(II) dodecahydrate
Chemical formula ^a	$6(\text{C}_{48}\text{H}_{24}\text{N}_4\text{NiO}_8^{4-})$, $18(\text{C}_{14}\text{H}_8\text{O}_6\text{S}^{2-})$, $5(\text{H}_4\text{O}_8\text{ZrO}_6^{12+})$, $12(\text{H}_2\text{O})$
Crystal system ^a	Cubic
Space group ^a	<i>Im-3m</i>
Unit cell dimensions ^a	a : $38.418(5)\text{ \AA}$, b : 38.418 \AA , c : 38.418 \AA ; α : 90.00° β : 90.00° γ : 90.0° V : 28351.39 \AA^3
Molecular volume ^a	$28,351.384\text{ \AA}^3$
Density (calc.) ^a	0.829 g cm^{-3}
Void volume ^b	65.6%
N_2 access. porosity ^b	0.25113(6)
He access. porosity ^c	0.40235(9)
N_2 access. volume ^c	0.32617(8)
He access. volume ^c	0.5226(1)
N_2 access. area ^c	2342.99(20)
LOS channel cross section diameter ^d	$\perp a$ -axis: $1.60\text{ \AA} \times 7.35\text{ \AA}$, oval

^aCambridge Center for Diffraction Data, 2019.

^bCalculated using Mercury 4.1.0, from the contact area of 1.2 \AA radius probe.

^cCalculated using model of Gelb and Gubbins (1999).

^dEstimated for 1.2 \AA probe using Mercury 4.1.0 graphics, Cambridge Centre for Diffraction Data, 2019.

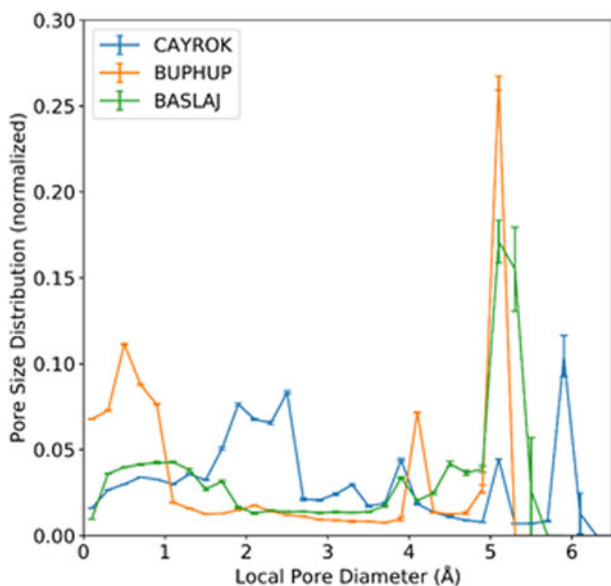


Figure 6. Pore-size distribution (PSD) in CAYROK, BUPHUP, and BASLAJ. Uncertainty is indicated by error bars, which correspond to 95% confidence intervals on the mean PSD computed via jackknife analysis of 10 replicate calculations for each material.

The LOS channel size is experimentally observed to accommodate disordered methanol or ethanol molecules with 1/3 occupancy per porphyrin formula unit (Deiters *et al.*, 2005). Similar results were obtained using cyclohexane as the solvent. For all three solvents, the solvent-free structure can be generated reversibly. No interactions with the channel walls were observed, although the fact that vacuum and heat must be applied for cyclohexane solvent removal implies that there may be a significant adsorption energy involved for this adsorbate. The conclusion is that this porphyrin is a robust porous material which can stably exist in the presence or absence of solvent. Crystallographic data are given in Table III.

TABLE III. Crystal data for pyridyldiphenyl zinc porphyrin (Deiters *et al.*, 2005).

Common name	Pyridyldiphenyl zinc porphyrin
CCDC symbol ^a	CAYROK
IUPAC name ^a	catena-(μ_3 -5,15-bis(4-Pyridyl)-10,20-diphenylporphyrin)-zinc)
Chemical formula ^a	(C ₄₂ H ₂₆ N ₆ Zn) _n
Crystal system ^a	Rhombohedral
Space group ^a	<i>R</i> -3
Unit cell dimensions ^a	<i>a</i> : 33.073(<1) Å, <i>b</i> : 33.073(<1) Å, <i>c</i> : 9.292(<1) Å; α : 90.00°, β : 90.00°, γ : 120.0°, <i>V</i> : 8802.422 Å ³
Molecular volume ^a	978.047 Å ³
Density (calc.) ^a	1.155 g cm ⁻³
Void volume ^b	18.1%
N ₂ access. porosity ^c	0.01425(2)
He access. porosity ^c	0.066286(4)
N ₂ access. volume ^c	0.012342(2) cm ³ g ⁻¹
He access. volume ^c	0.057409(4) cm ³ g ⁻¹
N ₂ access. area ^c	380.02(14) m ² g ⁻¹
LOS channel cross section diameter ^d	⊥ <i>c</i> -axis: 4.86 Å (minimum), 6.65 Å (maximum), star-shaped

^{a-d}Refer to Table II.

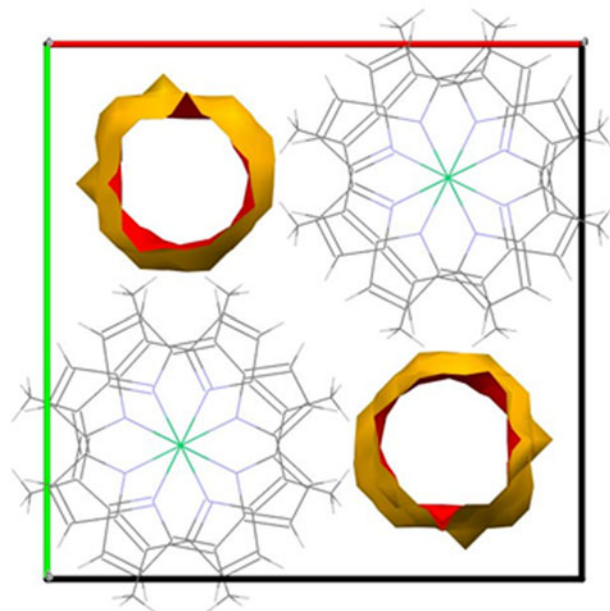


Figure 7. Channels in BUPHUP unit cell viewed down the *c*-axis.

C. Tetragonal (*P4/nnc*) tetramethyl porphyrin nickel iodide (BUPHUP)

BUPHUP is a porphyrinic compound which exhibits significant electrical conductivity. The structure was solved by Pace *et al.* (1983). Compositionally, the compound is similar to the iodine-free version, which differs compositionally in the lack of iodine; however, the iodine-free compound has a completely different structure and is non-conducting. In BUPHUP, the iodine resides in channels in disordered form as I₃⁻ chains parallel with the *c*-axis. The BUPHUP structure can be described without the iodine, but with the empty channels, as shown in Figure 7. The porphyrin molecules are in intimate contact with the exterior of the channel walls and are rotated at 45° to one another along the *c*-axis stacking direction.

TABLE IV. Crystal data for tetramethyl porphyrin nickel iodide (Pace *et al.*, 1983).

Common name	Tetramethyl porphyrin nickel iodide
CCDC symbol ^a	BUPHUP
IUPAC name ^a	(5,10,15,20-tetramethylporphyrinato)-nickel(ii) iodide
Chemical formula ^a	C ₂₄ H ₂₀ N ₄ Ni ⁺ , I ⁻
Crystal system ^a	Tetragonal
Space group ^a	<i>P4/nnc</i>
Unit cell dimensions ^a	<i>a</i> : 16.610(15) Å, <i>b</i> : 16.610(15) Å, <i>c</i> : 6.932(7) Å; α : 90.00°, β : 90.00°, γ : 90.00°, <i>V</i> : 1912.484 Å ³
Molecular volume ^a	478.121 Å ³
Density (calc.) ^a	1.91 g cm ⁻³
Void volume ^b	11.0%
N ₂ access. porosity ^c	0.00490(1)
He access. porosity ^c	0.03705(1)
N ₂ access. volume ^c	0.00333(1) cm ³ g ⁻¹
He access. volume ^c	0.02521(1) cm ³ g ⁻¹
N ₂ access. area ^c	147.10(11) m ² g ⁻¹
LOS channel cross section diameter ^d	⊥ <i>a</i> -axis: 3.88 Å, roughly circular

^{a-d}Refer to Table II.

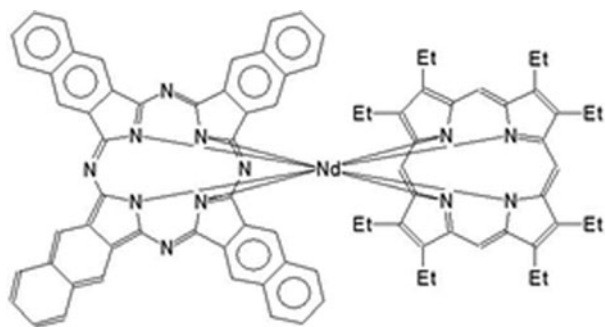


Figure 8. Schematic structural diagram of BASLAJ (Cambridge Center for Crystal Data, 2019).

The BUPHUP structure has a calculated void content of 11 volume %. In this structure, the Ni-metalated macrocycles are stacked over one another such that the Ni–Ni distance is 3.466 Å, considerably less than in the iodine-free version (5.648 Å) (Pace *et al.*, 1983). The macrocycles are not planar but rather have a saddle shape. The shortened stacking distance allows for π – π interaction, making one-dimensional (1D) conductivity along the c -axis possible, in conjunction with the I_3^- counterions in the adjacent channels. The average room-temperature electrical conductivity along the c -axis was measured as $110 \Omega^{-1}\text{cm}^{-1}$. At temperatures above ~ 115 K, where the maximum conductivity occurs, BUPHUP exhibits

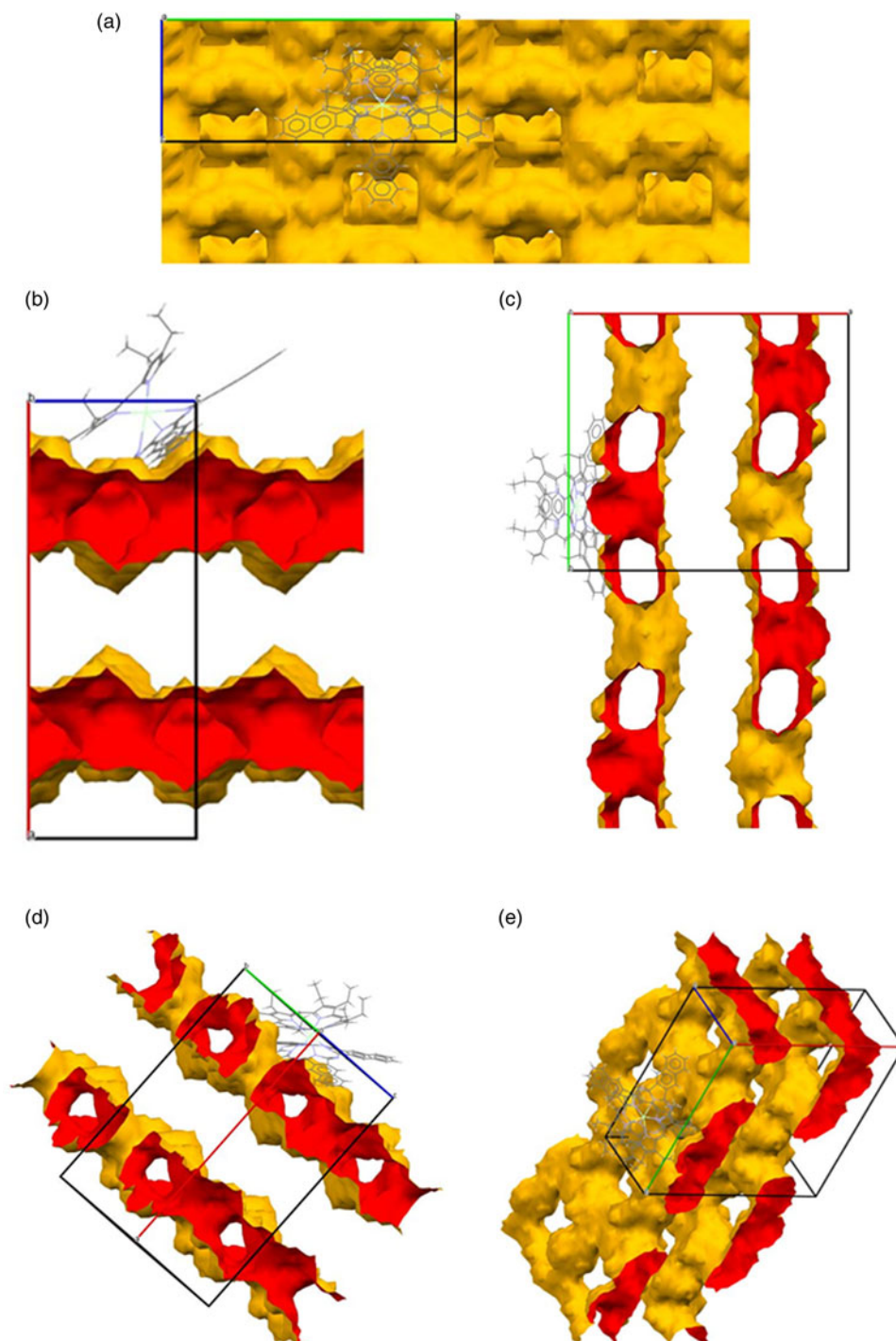


Figure 9. (a) Channels in BASLAJ viewed down the a -axis. (b) Channels in BASLAJ viewed down the b -axis. (c) Channels in BASLAJ viewed down the c -axis. (d) Channels in BASLAJ viewed down [011]. (e) Channels in BASLAJ viewed from an inclined perspective.

TABLE V. Crystal data for phthalocyanine-octaethyl porphyrin neodymium (Bian *et al.*, 2003).

Common name	Phthalocyanine-octaethyl porphyrin neodymium
CCDC symbol ^a	BASLAJ
IUPAC name ^a	(2,3-Naphthalocyaninato)-(2,3,7,8,12,13,17,18-octaethylporphyrinato)-neodymium(iii)
Chemical formula ^a	C ₈₄ H ₆₈ N ₁₂ Nd
Crystal system ^a	Orthorhombic
Space group ^a	<i>Pnma</i>
Unit cell dimensions ^a	<i>a</i> : 28.618(8) Å, <i>b</i> : 26.329(8) Å, <i>c</i> : 10.987(3) Å; α : 90.00°, β : 90.00°, γ : 90.00°, <i>V</i> : 8278.521 Å ³
Molecular volume ^a	2069.630 Å ³
Density (calculated) ^a	1.115 g cm ⁻³
Void volume ^b	25.7%
N ₂ access. porosity ^c	0.02533(2)
He access. porosity ^c	0.10481(6)
N ₂ access. volume ^c	0.02278(2) cm ³ g ⁻¹
He access. volume ^c	0.09426(6) cm ³ g ⁻¹
N ₂ access. area ^c	726.64(27) m ² g ⁻¹
LOS channel crosssection diameter ^d	⊥ <i>c</i> -axis: 3.80 Å × 6.58 Å, oval⊥ [011]: 2.86 Å × 2.99 Å, tear-drop

^{a-d}Refer to Table II.

metallic conductivity. The LOS channels along *c* have an approximately circular cross section with an average diameter of ~3.88 Å. The PSD, given in Figure 6, shows a strong peak at slightly above 5 Å. This correlates approximately with the main LOS channel and reflects the fact that the apparent LOS diameter is smaller than the undulations in the channel which are blocked from view in the LOS projection. As for CAYROK, the smaller pores indicated in the PSD are likely side pockets or cavities not part of the LOS channels. Whether the structure can exist as such without iodine is not known. Crystallographic properties are given in Table IV.

D. Orthorhombic (*Pnma*) naphthalocyanine-octaethyl porphyrin neodymium (BASLAJ)

Bian *et al.* (2003) determined the structure of a naphthalocyanine-octaethyl porphyrin, BASLAJ, in which the inner nitrogens of two parallel macrocycles are bonded to a central 8-coordinated neodymium atom, to form a sandwich motif, as shown diagrammatically in Figure 8. The two constituent macrocycles, one a phthalocyanine, the other a porphyrin, are closely related structurally and compositionally. The sandwiches pack together to form an orthorhombic molecular structure with a void content of 25.4 volume %.

The topology of the LOS channels formed by the packing differs as a function of crystallographic direction, due to the orthorhombic crystal symmetry. The length of the *c*-axis unit cell parameter is less than half of the *a*-axis and *b*-axis parameters; the latter are nearly equal. As viewed along the *a*-axis, there are no LOS channels observed (Figure 9(a)), rather the view is of the outer surface of a stack of two-dimensional (2D) sheets formed by grids of intersecting LOS channels perpendicular to this axis. The topology is evident in Figure 9(b), as viewed down the *b*-axis, where a longitudinal section of the LOS channels extending along *c* is illustrated. As viewed perpendicular to the *c*-axis (Figure 9(c)), the oval cross section of one set of the intersecting LOS channels is apparent, with projected LOS dimensions of ~3.80 Å by ~6.58 Å. The other set of intersecting LOS channels is visible if a section is taken perpendicular to [011], as in Figure 9(d); the cross section in this view indicates a tear-drop shape with dimensions of ~2.86 Å by ~2.99 Å. The roughly planar nature of the stacked channel grids is

clear in the inclined unit cell view of Figure 9(e). The PSD of BASLAJ, shown in Figure 6, indicates a predominant pore at 5.2 Å, which correlates with the LOS projection. The absence of other significant pores indicates that the free volume is dominated by channels, as suggested by the graphical representations in Figure 9. Crystallographic properties for BASLAJ are given in Table V.

Bian *et al.* (2003) were also able to study the crystallography of the lanthanide analogs (La, Pr, Tb, Dy, Ho, Er, Tm, Yb) and determined that all have the same crystallography as the Nd variant, thus suggesting the possibility of tuning optical and electronic properties by varying the rare earth composition. This could be useful for developing sensors which require the availability of open channels.

IV. DISCUSSION

The examples provided have diverse crystallographic structures, as illustrated by their calculated powder X-ray diffraction patterns (Figures 10(a)–10(d)). CAYROK, BUPHUP, and BASLAJ have a single strong line at 5°–7° two-theta, in accordance with their uniaxial or near-uniaxial (BASLAJ) character. The examples demonstrate that molecular porphyrins (e.g. BASLAJ), as well as porphyrinic MOF frameworks (e.g. BEPVIE), can have large porosities. Of particular interest are the channels in both types of structures. The close proximity of the metalated macrocycles to the channel walls creates the potential for a variety of host–guest interactions, such as the potential catalytic activity of BEPVIE and the electrical conductivity of BUPHUP. The open nature of the structures, enhanced by the presence of LOS channels, offers the opportunity for solid/gas and solid/liquid interactions of many types.

The entry and exit of adsorbates are central to applications, such as membranes, filters, sensors, molecular storage, ionic conduction, catalysis, and single-crystal-to-single-crystal guest exchange. In this regard, the reversible adsorbate phenomena observed in CAYROK warrants further discussion. By comparison of molecular diameters given in Table I with calculated channel diameters in Tables II–V, it is clear that larger adsorbates may be restricted in their movement in BEPVIE and BUPHUP. As confirmed by experimental observations (Deiters *et al.*, 2005), CAYROK, which has

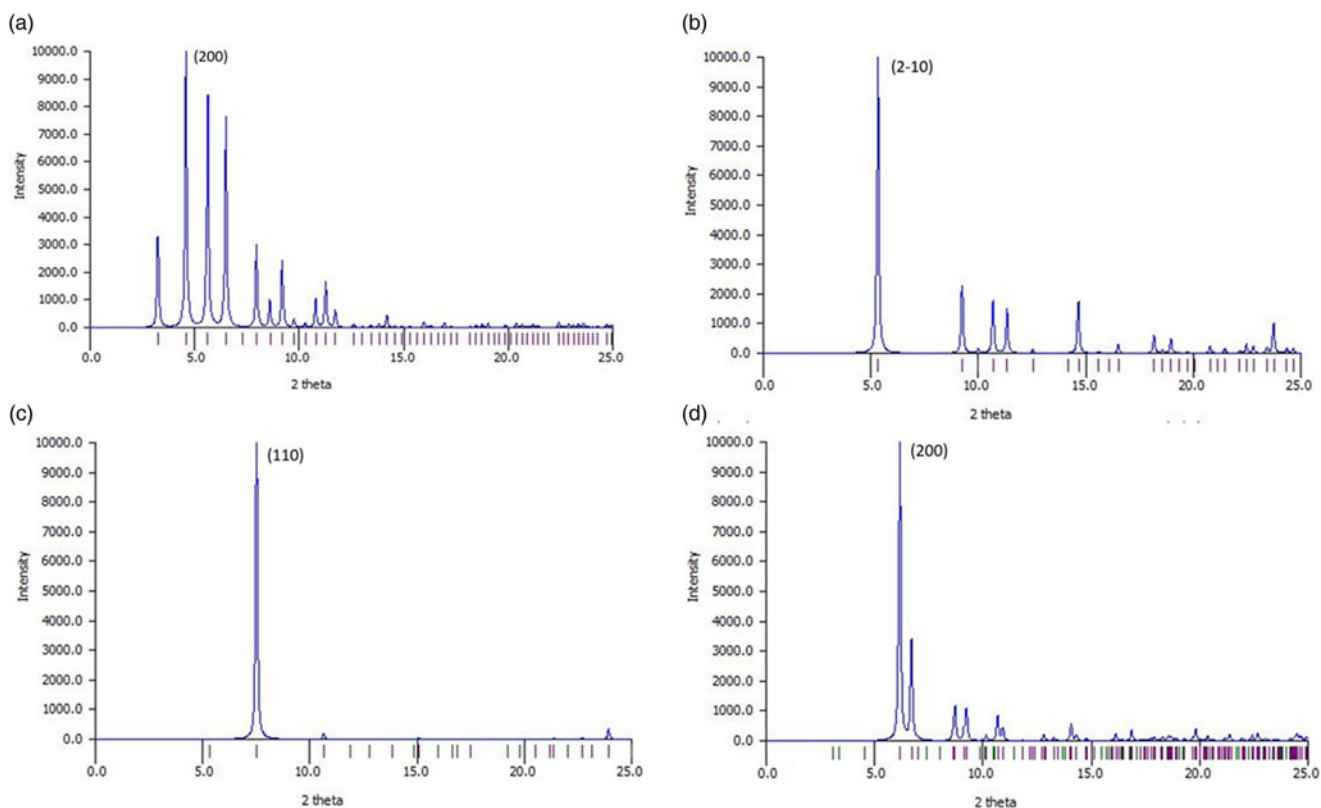


Figure 10. Calculated powder X-ray diffraction patterns for (a) BEPVIE, (b) CAYROK, (c) BUPHUP, (d) BASLAJ. $\text{CuK}\alpha$ radiation. Calculations were completed using Mercury 4.1.0.

LOS channels of $\sim 4.86\text{--}6.65$ Å diameter, readily accepts methanol (3.95 Å), and ethanol (4.50 Å). Cyclohexane (6.90 Å) required $7\times$ longer times, and a higher temperature of 50 °C, rather than room temperature, for the absorption/desorption process to fully occur. Since the channels are star-shaped, with a minimum effective circular diameter of ~ 4.86 Å, it is important to consider how the cyclohexane can enter, an issue not addressed by the original authors (Deiters *et al.*, 2005). An explanation can be derived by considering the shape and dynamic behavior of cyclohexane. The shape of the cyclic molecule is shown in side view in Figure 11, where it is clear in this orientation that the thickness is less than the length. Thus, the channel could be entered by the molecule in a sideways manner to take advantage of the maximum channel dimension of ~ 6.65 Å, with the equatorial hydrogens at the tips of the stars. The limiting molecular diameters are gradational in terms of electron density, and possibly channel-wall/molecule surface interaction could reduce the

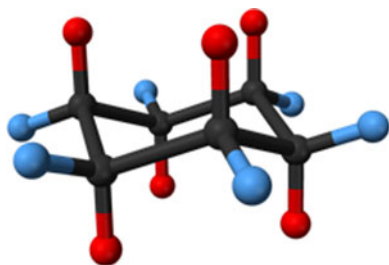


Figure 11. Cyclohexane, C_6H_{12} . Red = apical hydrogens, blue = equatorial hydrogens.

effective molecular diameter by a small amount, further facilitating entry. Also, the cyclohexane molecule is unstable in the perfectly planar state but rather exists in a dynamic state, rapidly alternating between four different bent ring conformations (Nelson and Brammer, 2011). Such motions could intermittently produce geometries favorable for entry. It is known that for pore diameters less than ~ 10 Å, diffusivity can change by several orders of magnitude because of relatively minor changes in the structure of the diffusing molecule (e.g. *cis*- versus *trans*-) or to minor changes in the channel diameter (Weisz, 1973).

Our focus has been mainly on LOS channels, as their diameter can be easily calculated and measured in cross section, and the migration of molecules through them is relatively straight forward. Other continuous, non-LOS channels can also accept absorbates, but the effect of tortuosity must be considered. In this case, dynamic interaction with wall curvatures and irregularities could have a large effect on the kinetics of motion along the channel. While the effect of tortuosity is important, we do not at present have an effective way of measuring tortuosity crystallographically.

V. CONCLUSIONS

We have completed calculations of voids in a randomly selected sample of 1000 of the ~ 8400 reported porphyrinic crystal structures in the CCDC organic database. Based on our calculations, several compounds have $>25\%$ void volume (for comparison, most simple salts and simple organics have negligible porosity). About 5% of the porphyrinic compounds have LOS continuous channels. Such materials have the

potential for advanced functional applications by utilizing the local molecular semiconducting properties of the porphyrin macrocycle in combination with the introduction of adsorbates having useful properties. From our random sample, we have highlighted four high-void-percentage examples with different crystallography and presented their detailed characterizations with respect to channel topology and pore-size distribution. Void topologies resulting from LOS channels with 1D, 2D, and 3D configurations were illustrated. Among these examples, we have noted possibilities for multi-metal catalysis, electrical conductivity, sensor applications, and selective adsorption/desorption. Further research on voids and channels in porphyrinic materials appears to be a promising avenue for future investigations.

- Bian, Y., Wang, D., Wang, R., Weng, L., Dou, J., Zhan, D., Ng, D. K. P., and Jiang, J. (2003). "Structural studies of the whole series of lanthanide double-decker compounds with mixed 2,3-naphthalocyaninato and octaethylporphyrinato ligands," *New J. Chem.* **27**, 844–849.
- Bondi, A. (1964). "Van der Waals volumes and radii," *J. Phys. Chem.* **68**(3), 441–451.
- Breck, D. W. (1974). *Zeolite Molecular Sieves: Structure, Chemistry, and Use* (Wiley, New York).
- Cambridge Crystallographic Data Centre. (2019). Available at <https://www.ccdc.cam.ac.uk/> (accessed on May–July).
- Cook, L. P., Wong-Ng, W., and Brewer, G. (2016). "Porphyrin-based chemistry for carbon capture and sequestration," in *Advances in Materials Science for Environmental and Energy Technologies V*, edited by T. Ohji, R. Kanakhala, J. Matyáš, N. Marijooran, G. Pickrell, and W. Wong-Ng (Wiley & Sons, Hoboken, NJ), pp. 201–221.
- Cook, L. P., Brewer, G., and Wong-Ng, W. (2017). "Structural aspects of porphyrins for functional materials applications," *Crystals*. **7**(7), 223.
- Crossley, M. J. and Burn, P. L. (1991). "An approach to porphyrin-based molecular wires: synthesis of a bis(porphyrin)tetraone and its conversion to a linearly conjugated tetrakisporphyrin system," *Chem. Commun.* **1991**, 1569–1571.
- Deiters, E., Bulach, V., and Hosseini, M. W. (2005). "Reversible single-crystal to single-crystal guest exchange in a 3-D coordination network based on a zinc porphyrin," *Chem. Commun.* **2005**, 3906–3908.
- Duren, T., Millange, F., Ferey, G., Walton, K. S., and Snurr, R. Q. (2007). "Calculating geometric surface areas as a characterization tool for metal–organic frameworks," *J. Phys. Chem. C*. **111**, 15350.
- Frost, H., Duren, T., and Snurr, R. Q. (2006). "Effects of surface area, free volume, and heat of adsorption on hydrogen uptake in metal–organic frameworks," *J. Phys. Chem. B*. **110**, 9565.
- Galloni, P., Vecchi, A., Coletti, A., Gatto, E., Floris, B., and Conte, V. (2014). "Porphyrins as active components for electrochemical and photoelectrochemical devices," in *Handbook of Porphyrin Science*, Volume 33, edited by W. Kadish, K. M. Smith, and R. Guilard (World Scientific Publishing Co., Singapore), pp. 225–415.
- Gao, C., Shi, Q., and Dong, J. (2016). "Adsorptive separation performance of 1-butanol onto typical hydrophobic zeolitic imidazolate frameworks (ZIFs)," *CrystEngComm*. **18**, 3842–3849.
- Gelb, L. D. and Gubbins, K. E. (1999). "Pore size distributions in porous glasses: a computer simulation study," *Langmuir*. **15**(2), 305–308.
- Ismail, A. F., Khulbe, K., and Matsuura, T. (2015). *Gas Separation Membranes: Polymeric and Inorganic* (Springer, New York, NY).
- Jiang, Y.-B. and Sun, Z. (2019). "Self-assembled porphyrin and macrocycle derivatives: from synthesis to function," *Mater. Res. Bull.* **44**(3), 167–171.
- Jones, R., Tredgold, R. H., and Hoorfar, A. (1984). "Electrical conductivity in Langmuir-Blodgett films of porphyrins: in-plane and through-the-film studies," *Thin Solid Films*. **113**, 115–118.
- Jurow, M., Schuckman, A., Batteas, J. D., and Drain, C. M. (2010). "Porphyrins as molecular components of functional devices," *Coordination Chem. Rev.* **254**, 2297–2310.
- Kadish, K. M., Smith, K. M., and Guilard, R. (2010–2019). *Handbook of Porphyrin Science* (World Scientific, Hackensack, NJ).
- Li, J.-M. and Talu, O. (1993). "Effect of structural heterogeneity on multicomponent adsorption: benzene and p-xylene mixture on silicalite," in *Fundamentals of Adsorption*, edited by M. Suzuki (Elsevier, Amsterdam), pp. 373–380.
- Matteucci, S., Yampolskii, Y., Freeman, B. D., and Pinneau, I. (2006). "Materials science of membranes for gas and vapor separation," in *Materials Science of Membranes for Gas and Vapor Separation*, edited by Y. Yampolskii, B. D. Freeman and I. Pinneau (John Wiley and Sons, West Sussex, England), pp. 1–47.
- Nelson, D. J. and Brammer, C. N. (2011). "Toward consistent terminology for cyclohexane conformers in introductory organic chemistry," *J. Chem. Educ.* **88**(3), 292–294.
- Nguyen, H. G., Horn, J. C., Bleakney, M., Siderius, D. W., and Espinal, L. (2019). "Understanding material characteristics through signature traits from helium pycnometry," *Langmuir*. **35**(6), 2115–2122.
- Pace, L. J., Martinsen, J., Ulman, A., Hoffman, B. M., and Ibers, J. A. (1983). "Conductive molecular crystals. Structural, magnetic, and charge-transport properties of (5,10,15,20-Tetramethylporphyrinato)nickel(II) iodide," *J. Am. Chem. Soc.* **105**, 2612–2620.
- Palmer, J. C., Moore, J. D., Brennan, J. K., and Gubbins, K. E. (2011). "Simulating local adsorption isotherms in structurally complex porous materials: a direct assessment of the slit pore model," *J. Phys. Chem. Lett.* **2**(3), 165–169.
- Rowland, R. S. and Taylor, R. (1996). "Intermolecular nonbonded contact distances in organic crystal structures: comparison with distances expected from van der Waals Radii," *J. Phys. Chem.* **100**(18), 7384–7391.
- Suslick, K. S., Rakow, N. A., Kosal, M. E., and Chou, J. H. (2000). "The materials chemistry of porphyrins and metalloporphyrins," *J. Porphyr. Phthalocyanines*. **4**, 407–413.
- Walton, K. S. and Snurr, R. Q. (2007). "Applicability of the BET method for determining surface areas of microporous metal–organic frameworks," *J. Am. Chem. Soc.* **129**, 8552–8556.
- Weisz, P. B. (1973). "Zeolites – new horizons in catalysis," *Chemtech*. **3**, 498–505.
- Wong-Ng, W., Kaduk, J. A., Wu, H., and Suchomel, M. (2012). "Synchrotron X-ray studies of metal-organic framework $M_2(2,5\text{-dihydroxyterephthalate})$, $M=(Mn,Co,Ni,Zn)$ (MOF74)," *Powder Diffr.* **27**(4), 256–262.
- Wong-Ng, W., Culp, J. T., Chen, Y. S., Zavalij, P., Espinal, L., Siderius, D. W., Allen, A. J., Scheins, S., and Matranga, C. (2013). "Improved synthesis and crystal structure of the flexible pillared layer porous coordination polymer: Ni(1,2-bis(4-pyridyl)ethylene)[Ni(CN)₄]," *CrystEngComm*. **15**, 4684–4693.
- Wong-Ng, W., Kaduk, J. A., Siderius, D. L., Allen, A. L., Espinal, L., Boyerinas, B. M., Levin, I., Suchomel, M. R., Ilavsky, J., Li, L., Williamson, I., Cockayne, E., and Wu, H. (2015). "Reference diffraction patterns, microstructure, and pore size distribution for the copper (II) benzene-1,3,5-tricarboxylate metal organic framework (Cu-BTC) compounds," *Powder Diffr.* **30**(1), 2–13.
- Wong-Ng, W., Williamson, I., Lawson, M., Siderius, D. W., Culp, J. T., Chen, Y.-S., and Li, L. (2018). "Electronic structure, pore size distribution, and sorption characterization of an unusual MOF, {[Ni(dpbz)][Ni(CN)₄]}_n, dpbz=1,4-bis(4-pyridyl)benzene," *J. Appl. Phys.* **123**, 245104.
- Wong-Ng, W., Nguyen, H. G., Espinal, L., Siderius, D. W., and Kaduk, J. A. (2019). "Powder X-ray structural studies and reference diffraction patterns for three forms of porous aluminum terephthalate, MIL-53(A1)," *Powder Diffr.* **34**(3), 216–226.
- Yuan, S., Qin, J.-S., Li, J., Huang, L., Feng, L., Fang, Y., Lollar, C., Pang, J., Zhang, L., Sun, D., Alsalmeh, A., Cagin, T., and Zhou, H.-C. (2018). "Retrosynthesis of multi-component metal-organic frameworks," *Nat. Commun.* **9**, 808.